

# Symbolic-Numeric Algorithms for Computer Analysis of Spheroidal Quantum Dot Models

A.A. Gusev<sup>1,2</sup>, O. Chuluunbaatar<sup>1</sup>, V.P. Gerdt<sup>1</sup>, V.A. Rostovtsev<sup>1,2</sup>,  
S.I. Vinitsky<sup>1</sup>, V.L. Derbov<sup>3</sup>, V.V. Serov<sup>3</sup>

<sup>1</sup> Joint Institute for Nuclear Research, Dubna, Russia

<sup>2</sup> Dubna International University of Nature, Society & Man, Dubna, Russia

<sup>3</sup> Saratov State University, Saratov, Russia

gooseff@jinr.ru

**Abstract.** A computational scheme for solving elliptic boundary value problems with axially symmetric confining potentials using different sets of one-parameter basis functions is presented. The efficiency of the proposed symbolic-numerical algorithms implemented in Maple is shown by examples of spheroidal quantum dot models, for which energy spectra and eigenfunctions versus the spheroid aspect ratio were calculated within the conventional effective mass approximation. Critical values of the aspect ratio, at which the discrete spectrum of models with finite-wall potentials is transformed into a continuous one in strong dimensional quantization regime, were revealed using the exact and adiabatic classifications.

## 1 Introduction

To analyze the geometrical, spectral and optical characteristics of quantum dots in the effective mass approximation and in the regime of strong dimensional quantization following [1], many methods and models were used, including the exactly solvable model of a spherical impermeable well [2], the adiabatic approximation for a lens-shaped well confined to a narrow wetting layer [3] and a hemispherical impermeable well [4], the model of strongly oblate or prolate ellipsoidal impermeable well [5], as well as numerical solutions of the boundary value problems (BVPs) with separable variables in the spheroidal coordinates for wells with infinite and finite wall heights [6,7,8]. However, thorough comparative analysis of spectral characteristics of models with different potentials, including those with non-separable variables, remains to be a challenging problem. This situation stimulates the study of a wider class of model well potentials with application of symbolic-numerical algorithms (SNA) and problem-oriented software developed by the authors of the present paper during years [9,10,11,12,13,14].

Here we analyse the spectral characteristics of the following models: a spherical quantum dot (SQD), an oblate spheroidal quantum dot (OSQD), and a prolate spheroidal quantum dot (PSQD). We make use of the Kantorovich method that reduces the problem to a set of ordinary differential equations (ODE) [15]. In contrast to the well-known method of adiabatic representation [16], this method

implies neither adiabatic separation of fast and slow variables nor the presence of a small parameter. We present a calculation scheme for solving elliptical BVPs with axially-symmetric potentials in cylindrical coordinates (CC), spherical coordinates (SC), oblate spheroidal coordinates (OSC), and prolate spheroidal coordinates (PSC). Basing on the SNA developed for axially-symmetric potentials, different sets of solutions are constructed for the parametric BVPs related to the fast subsystem, namely, the eigenvalue problem solutions (the terms and the basis functions), depending upon the slow variable as a parameter, as well as the matrix elements, i.e., the integrals of the products of basis functions and their derivatives with respect to the parameter, which are calculated analytically by means of elaborated SNA MATRA implemented in MAPLE, or numerically using the program ODPEVP [13] implementing the finite-element method (FEM). These terms and matrix elements form the matrices of variable coefficients in the set of second-order ODE with respect to the slow variable. The BVP for this set of ODEs is solved by means of the program KANTBP [11], also implementing the FEM. The efficiency of the calculation scheme and the SNA used is demonstrated by comparison of the spectra versus the ellipticity of the prolate or oblate spheroid in the models of quantum dots with different confining potentials, such as the isotropic and anisotropic harmonic oscillator, the spherical and spheroidal well with finite or infinite walls approximated by smooth short-range potentials as well as by constructing the adiabatic classification of the states.

The paper is organized as follows. In Section 2, the calculation scheme for solving elliptic BVPs with axially-symmetric confining potentials is presented. In Section 3, SNA MATRA for solving parametric BVP and corresponding integrals implemented in Maple is described. Section 4 is devoted to the analysis of the spectra of quantum dot models with three types of axially-symmetric potentials, including the benchmark exactly solvable models. In Conclusion we summarize the results and discuss the future applications of our calculation scheme and the SNA project presented.

## 2 Problem Statement

Within the effective mass approximation under the conditions of strong dimensional quantization, the Schrödinger equation for the slow envelope of the wave function  $\tilde{\Psi}(\tilde{\mathbf{r}})$  of a charge carrier (electron  $e$  or hole  $h$ ) in the models of a spherical, prolate or oblate spheroidal quantum dot (SQD, PSQD or OSQD) has the form

$$\{\tilde{H} - \tilde{E}\}\tilde{\Psi}(\tilde{\mathbf{r}}) = \{(2\mu_p)^{-1}\tilde{\mathbf{P}}^2 + \tilde{U}(\tilde{\mathbf{r}}) - \tilde{E}\}\tilde{\Psi}(\tilde{\mathbf{r}}) = 0, \quad (1)$$

where  $\tilde{\mathbf{r}} \in \mathbf{R}^3$  is the position vector of the particle having the effective mass  $\mu_p = \mu_e$  (or  $\mu_p = \mu_h$ ),  $\tilde{\mathbf{P}} = -i\hbar\nabla_{\tilde{\mathbf{r}}}$  is the momentum operator,  $\tilde{E}$  is the energy of the particle,  $\tilde{U}(\tilde{\mathbf{r}})$  is the axially-symmetric potential confining the particle motion in SQD, PSQD or OSQD. In Model A,  $\tilde{U}(\tilde{\mathbf{r}})$  is chosen to be the potential of an

isotropic or anisotropic axially-symmetric harmonic oscillator with the angular frequency  $\tilde{\omega} = \gamma_{\tilde{r}_0} \hbar / (\mu_p \tilde{r}_0^2)$ ,  $\gamma_{\tilde{r}_0} \sim \pi^2/3$  being an adjustable parameter:

$$\tilde{U}^L(\tilde{\mathbf{r}}) = \mu_p \tilde{\omega}^2 (\zeta_1 (\tilde{x}^2 + \tilde{y}^2) + \zeta_3 \tilde{z}^2) / 2, \quad (2)$$

$r_0 = \sqrt{\zeta_1 (\tilde{x}_0^2 + \tilde{y}_0^2) + \zeta_3 \tilde{z}_0^2}$  is the radius of a spherical QD ( $\zeta_1 = 1, \zeta_3 = 1$ ) or that of a spheroidal QD ( $\zeta_1 = (\tilde{r}_0/\tilde{a})^4, \zeta_3 = (\tilde{r}_0/\tilde{c})^4$ ), inscribed into a spherical one, where  $\tilde{a}$  and  $\tilde{c}$  are the semiaxes of the ellipse which transforms into a sphere at  $\tilde{a} = \tilde{c} = \tilde{r}_0$ . For Model B,  $\tilde{U}(\tilde{\mathbf{r}})$  is the potential of a spherical or axially-symmetric well

$$\tilde{U}^B(\tilde{\mathbf{r}}) = \{0, 0 \leq (\tilde{x}^2 + \tilde{y}^2)/\tilde{a}^2 + \tilde{z}^2/\tilde{c}^2 < 1; \tilde{U}_0, (\tilde{x}^2 + \tilde{y}^2)/\tilde{a}^2 + \tilde{z}^2/\tilde{c}^2 \geq 1\}, \quad (3)$$

with walls of finite or infinite height  $1 \ll \tilde{U}_0 < \infty$ . For Model C,  $\tilde{U}(\tilde{\mathbf{r}})$  is taken to be a spherical or axially-symmetric diffuse potential

$$\tilde{U}^C(\tilde{\mathbf{r}}) = \tilde{U}_0 [1 + \exp(((\tilde{x}^2 + \tilde{y}^2)/\tilde{a}^2 + \tilde{z}^2/\tilde{c}^2 - 1)/s)]^{-1}, \quad (4)$$

where  $s$  is the edge diffusiveness parameter of the function smoothly approximating the vertical walls of finite height  $\tilde{U}_0$ . Below we restrict ourselves by considering Model B with infinite walls  $\tilde{U}_0 \rightarrow \infty$  and Model C with walls of finite height  $\tilde{U}_0$ . We make use of the reduced atomic units:  $a_B^* = \kappa \hbar^2 / \mu_p e^2$  is the reduced Bohr radius,  $\kappa$  is the DC permittivity,  $E_R \equiv Ry^* = \hbar^2 / (2\mu_p a_B^{*2})$  is the reduced Rydberg unit of energy, and the following dimensionless quantities are introduced:  $\tilde{\Psi}(\tilde{\mathbf{r}}) = a_B^{*-3/2} \Psi(\mathbf{r})$ ,  $2\hat{H} = \hat{H}/Ry^*$ ,  $2E = \tilde{E}/Ry^*$ ,  $2U(\mathbf{r}) = \tilde{U}(\tilde{\mathbf{r}})/Ry^*$ ,  $\mathbf{r} = \tilde{\mathbf{r}}/a_B^*$ ,  $a = \tilde{a}/a_B^*$ ,  $\tilde{c} = c/a_B^*$ ,  $r_0 = \tilde{r}_0/a_B^*$ ,  $\omega = \gamma_{r_0}/r_0^2 = \hbar\tilde{\omega}/(2Ry^*)$ . For an electron with the reduced mass  $\mu_p \equiv \mu_e = 0.067m_0$  at  $\kappa = 13.18$  in GaAs:  $a_B^* = 102\text{\AA} = 10.2 \text{ nm}$ ,  $Ry^* = E_R = 5.2 \text{ meV}$ .

Since the Hamiltonian  $\hat{H}$  in (1)–(4) commutes with the  $z$ -parity operator ( $z \rightarrow -z$  or  $\eta \rightarrow -\eta$ ), the solutions are divided into even ( $\sigma = +1$ ) and odd ( $\sigma = -1$ ) ones. The solution of Eq. (1), periodical with respect to the azimuthal angle  $\varphi$ , is sought in the form of a product  $\Psi(x_f, x_s, \varphi) = \Psi^{m\sigma}(x_f, x_s) e^{im\varphi} / \sqrt{2\pi}$ , where  $m = 0, \pm 1, \pm 2, \dots$  is the magnetic quantum number. Then the function  $\Psi^{m\sigma}(x_f, x_s)$  satisfies the following equation in the two-dimensional domain  $\Omega = \Omega_{x_f}(x_s) \cup \Omega_{x_s} \subset \mathbf{R}^2 \setminus \{0\}$ ,  $\Omega_{x_f}(x_s) = (x_f^{\min}(x_s), x_f^{\max}(x_s))$ ,  $\Omega_{x_s} = (x_s^{\min}, x_s^{\max})$ :

$$\left( \hat{H}_1(x_f; x_s) + \hat{H}_2(x_s) + V(x_f, x_s) - 2E \right) \Psi^{m\sigma}(x_f, x_s) = 0. \quad (5)$$

The Hamiltonian of the slow subsystem  $\hat{H}_2(x_s)$  is expressed as

$$\hat{H}_2(x_s) = \check{H}_2(x_s) = -\frac{1}{g_{1s}(x_s)} \frac{\partial}{\partial x_s} g_{2s}(x_s) \frac{\partial}{\partial x_s} + \check{V}_s(x_s), \quad (6)$$

and the Hamiltonian of the fast subsystem  $\hat{H}_1(x_f; x_s)$  is expressed via the reduced Hamiltonian  $\check{H}_f(x_f; x_s)$  and the weighting factor  $g_{3s}(x_s)$ :

$$\begin{aligned} \hat{H}_1(x_f; x_s) &= g_{3s}^{-1}(x_s) \check{H}_f(x_f; x_s), \\ \check{H}_f(x_f; x_s) &= -\frac{1}{g_{1f}(x_f)} \frac{\partial}{\partial x_f} g_{2f}(x_f) \frac{\partial}{\partial x_f} + \check{V}_f(x_f) + \check{V}_{fs}(x_f, x_s). \end{aligned} \quad (7)$$

**Table 1.** The values of conditionally fast  $x_f$  and slow  $x_s$  independent variables, the coefficients  $g_{is}(x_s)$ ,  $g_{jf}(x_f)$ , and the potentials  $\check{V}_f(x_f)$ ,  $\check{V}_s(x_s)$ ,  $\check{V}_{fs}(x_f, x_s)$ , in Eqs.(5)–(7) for SQD, OSQD and PSQD in cylindrical (CC), spherical (SC), and oblate & prolate spheroidal (OSC & PSC) coordinates with  $(d/2)^2 = \pm(a^2 - c^2)$ , + for OSC, – for PSC.

	CC		SC	OSC & PSC
	OSQD	PSQD	SQD	OSQD & PSQD
$x_f$	$z$	$\rho$	$\eta$	$\eta$
$x_s$	$\rho$	$z$	$r$	$\xi$
$g_{1f}$	1	$\rho$	1	1
$g_{2f}$	1	$\rho$	$1 - \eta^2$	$1 - \eta^2$
$g_{1s}$	$\rho$	1	$r^2$	1
$g_{2s}$	$\rho$	1	$r^2$	$\xi^2 \pm 1$
$g_{3s}$	1	1	$r^2$	1
$\check{V}_f(x_f)$	$\omega^2 \zeta_3 z^2$	$m^2/\rho^2 + \omega^2 \zeta_1 \rho^2$	$m^2/g_{2f}$	$m^2/g_{2f} \pm (d/2)^2 g_{2f} 2E$
$\check{V}_s(x_s)$	$m^2/\rho^2 + \omega^2 \zeta_1 \rho^2$	$\omega^2 \zeta_3 z^2$	0	$\mp m^2/g_{2s} - ((d/2)^2 g_{2s} - 1) 2E$
$\check{V}_{fs}(x_f, x_s)$	0	0	$\check{V}(r, \eta)$	$V(\xi, \eta)$

Table 1 contains the values of conditionally fast  $x_f$  and slow  $x_s$  independent variables, the coefficients  $g_{1s}(x_s)$ ,  $g_{2s}(x_s)$ ,  $g_{3s}(x_s)$ ,  $g_{1f}(x_f)$ ,  $g_{2f}(x_f)$ , and the reduced potentials  $\check{V}_f(x_f)$ ,  $\check{V}_s(x_s)$ ,  $\check{V}_{fs}(x_f, x_s)$ , entering Eqs. (5)–(7) for SQD, OSQD, and PSQD in cylindrical ( $\mathbf{x} = (z, \rho, \varphi)$ ), spherical ( $\mathbf{x} = (r, \eta = \cos \theta, \varphi)$ ), and oblate/prolate spheroidal ( $\mathbf{x} = (\xi, \eta, \varphi)$ ) coordinates [17]. In spherical coordinates, the potential  $\check{V}(r, \eta)$  in Table 1 using the definitions (2), (4) in the reduced atomic units, for Model A is expressed as

$$\check{V}(r, \eta) = 2r^2 V(r, \eta) = \omega^2 r^4 (\zeta_1 (1 - \eta^2) + \zeta_3 \eta^2),$$

and for Model C as

$$\check{V}(r, \eta) = 2r^2 V(r, \eta) = 2r^2 U_0 [1 + \exp((r^2((1 - \eta^2)/a^2 + \zeta_3 \eta^2/c^2) - 1)/s)]^{-1},$$

both having zero first derivatives in the vicinity of the origin  $r = 0$  (equilibrium point). For Model B. the potentials  $\check{V}_{fs}$  are zero, since the potential (3) is reformulated below in the form of boundary conditions with respect to the variables  $x_f$  and  $x_s$ . The solution  $\Psi_i^{m\sigma}(x_f, x_s) \equiv \Psi_i^{Em\sigma}(x_f, x_s)$  of the problem (5)–(7) is sought in the form of Kantorovich expansion [15]

$$\Psi_i^{Em\sigma}(x_f, x_s) = \sum_{j=1}^{j_{\max}} \Phi_j^{m\sigma}(x_f; x_s) \chi_j^{(m\sigma i)}(E, x_s), \quad (8)$$

using as a set of trial functions the eigenfunctions  $\Phi_j^{m\sigma}(x_f; x_s)$  of the Hamiltonian  $\check{H}_f(x_f; x_s)$  from (7), i.e., the solutions of the parametric BVP

$$\{\check{H}_f(x_f; x_s) - \check{\lambda}_i(x_s)\} \Phi_i^{m\sigma}(x_f; x_s) = 0, \quad (9)$$

in the interval  $x_f \in \Omega_{x_f}(x_s)$  depending on the conditionally slow variable  $x_s \in \Omega_{x_s}$  as on a parameter. These solutions obey the boundary conditions

$$\lim_{x_f \rightarrow x_f^t(x_s)} \left( N_f^{(m\sigma)}(x_s) g_{2f}(x_f) \frac{d\Phi_j^{m\sigma}(x_f; x_s)}{dx_f} + D_f^{(m\sigma)}(x_s) \Phi_j^{m\sigma}(x_f; x_s) \right) = 0 \quad (10)$$

at the boundary points  $\{x_f^{\min}(x_s), x_f^{\max}(x_s)\} = \partial\Omega_{x_f}(x_s)$ , of the interval  $\Omega_{x_f}(x_s)$ . In Eq. (10),  $N_f^{(m\sigma)}(x_s) \equiv N_f^{(m\sigma)}$ ,  $D_f^{(m\sigma)}(x_s) \equiv D_f^{(m\sigma)}$ , unless specially declared, are determined by the relations  $N_f^{(m\sigma)} = 1$ ,  $D_f^{(m\sigma)} = 0$  at  $m = 0$ ,  $\sigma = +1$  (or at  $\sigma = 0$ , i.e., without parity separation),  $N_f^{(m\sigma)} = 0$ ,  $D_f^{(m\sigma)} = 1$  at  $m = 0$ ,  $\sigma = -1$  or at  $m \neq 0$ . The eigenfunctions satisfy the orthonormality condition with the weighting function  $g_{1f}(x_f)$  in the same interval  $x_f \in \Omega_{x_f}(x_s)$ :

$$\langle \Phi_i^{m\sigma} | \Phi_j^{m\sigma} \rangle = \int_{x_f^{\min}(x_s)}^{x_f^{\max}(x_s)} \Phi_i^{m\sigma}(x_f; x_s) \Phi_j^{m\sigma}(x_f; x_s) g_{1f}(x_f) dx_f = \delta_{ij}. \quad (11)$$

Here  $\tilde{\lambda}_1(x_s) < \dots < \tilde{\lambda}_{j_{\max}}(x_s) < \dots$  is the desired set of real eigenvalues. The corresponding set of potential curves  $2E_1(x_s) < \dots < 2E_{j_{\max}}(x_s) < \dots$  of Eqs. (7) is determined by  $2E_j(x_s) = g_{3s}^{-1}(x_s) \tilde{\lambda}_j(x_s)$ . Note that for OSC and PSC, the desired set of real eigenvalues  $\tilde{\lambda}_j(x_s)$  depends on a combined parameter,  $x_s \rightarrow p^2 = (d/2)^2 2E$ , the product of spectral  $2E$  and geometrical  $(d/2)^2$  parameters of the problem (5). The solutions of the problem (9)–(11) for Models A and B are calculated in the analytical form, while for Model C this is done using the program ODPEVP [13].

Substituting the expansion (8) into Eq. (5) in consideration of (9) and (11), we get a set of ODEs for the slow subsystem with respect to the unknown vector functions  $\chi^{(m\sigma i)}(x_s, E) \equiv \chi^{(i)}(x_s) = (\chi_1^{(i)}(x_s), \dots, \chi_{j_{\max}}^{(i)}(x_s))^T$ :

$$\begin{aligned} & \left( -\frac{1}{g_{1s}(x_s)} \mathbf{I} \frac{d}{dx_s} g_{2s}(x_s) \frac{d}{dx_s} + 2\mathbf{E}(x_s) + \mathbf{I} \tilde{V}_s(x_s) - 2\mathbf{I}E \right) \chi^{(i)}(x_s) = \\ & = -\left( \frac{g_{2s}(x_s)}{g_{1s}(x_s)} \mathbf{W}(x_s) + \frac{1}{g_{1s}(x_s)} \frac{dg_{2s}(x_s) \mathbf{Q}(x_s)}{dx_s} + \frac{g_{2s}(x_s)}{g_{1s}(x_s)} \mathbf{Q}(x_s) \frac{d}{dx_s} \right) \chi^{(i)}(x_s). \end{aligned} \quad (12)$$

Here  $2\mathbf{E}(x_s) = \text{diag}(g_{3s}^{-1}(x_s) \tilde{\lambda}_j(x_s))$ ,  $\mathbf{W}(x_s)$ , and  $\mathbf{Q}(x_s)$  are matrices of the dimension  $j_{\max} \times j_{\max}$ ,

$$\begin{aligned} W_{ij}(x_s) &= W_{ji}(x_s) = \int_{x_f^{\min}(x_s)}^{x_f^{\max}(x_s)} g_{1f}(x_f) \frac{\partial \Phi_i(x_f; x_s)}{\partial x_s} \frac{\partial \Phi_j(x_f; x_s)}{\partial x_s} dx_f, \\ Q_{ij}(x_s) &= -Q_{ji}(x_s) = - \int_{x_f^{\min}(x_s)}^{x_f^{\max}(x_s)} g_{1f}(x_f) \Phi_i(x_f; x_s) \frac{\partial \Phi_j(x_f; x_s)}{\partial x_s} dx_f, \end{aligned} \quad (13)$$

calculated analytically for Model B and by means of the program ODPEVP [13] for Model C. Note that for Model A in SC or CC and Model B in OSC or PSC, the variables  $x_f$  and  $x_s$  are separated so that the matrix elements  $W_{ij}(x_s) = Q_{ij}(x_s) \equiv 0$  are put into the r.h.s. of Eq. (12), and  $\tilde{V}_s(x_s)$  are substituted from Table 1. The discrete spectrum solutions  $2E : 2E_1 < 2E_2 < \dots < 2E_t < \dots$  that obey the boundary conditions at points  $x_s^t = \{x_s^{\min}, x_s^{\max}\} = \partial\Omega_{x_s}$  bounding the interval  $\Omega_{x_s}$ :

$$\lim_{x_s \rightarrow x_s^t} \left( N_s^{(m\sigma)} g_{2s}(x_s) \frac{d\chi^{(m\sigma p)}(x_s)}{dx_s} + D_s^{(m\sigma)} \chi^{(m\sigma p)}(x_s) \right) = 0, \quad (14)$$

where  $N_s^{(m\sigma)} = 1$ ,  $D_s^{(m\sigma)} = 0$  at  $m = 0, \sigma = +1$  (or at  $\sigma = 0$ , i.e. without parity separation),  $N_s^{(m\sigma)} = 0$ ,  $D_s^{(m\sigma)} = 1$  at  $m = 0, \sigma = -1$  or at  $m \neq 0$ , and the orthonormality conditions

$$\int_{x_s^{\min}}^{x_s^{\max}} (\chi^{(i)}(x_s))^T \chi^{(j)}(x_s) g_{1s}(x_s) dx_s = \delta_{ij}, \quad (15)$$

are calculated by means of the program KANTBP [11]. To ensure the prescribed accuracy of calculation of the lower part of the spectrum discussed below with eight significant digits we used  $j_{\max} = 16$  basis functions in the expansion (8) and the discrete approximation of the desired solution by Lagrange finite elements of the fourth order with respect to the grid pitch  $\Omega_{h^s(x_s)}^p = [x_{\min}^s, x_k^s = x_{k-1}^s + h_k^s, x_{\max}^s]$ .

### 3 SNA MATRA for Calculation of the BVP and Integrals

To calculate the effective potentials of the problem (12)–(15) for each value  $x_s = x_k^s$  of the FEM grid  $\Omega_{h^s(x_s)}^p = [x_{\min}^s, x_{\max}^s]$  we consider a discrete representation of solutions  $\Phi(x_f; x_s) \equiv \Phi^{m\sigma}(x_f; x_s)$  of the problem (9) by means of the FEM on the grid,  $\Omega_{h^f(x_f)}^p(x_s) = [x_0^f = x_{\min}^f(x_s), x_k^f = x_{k-1}^f + h_k^f, x_{\bar{n}}^f = x_{\max}^f(x_s)]$ , in a finite sum:

$$\Phi(x_f; x_s) = \sum_{\mu=0}^{\bar{n}p} \Phi_{\mu}^h(x_s) N_{\mu}^p(x_f) = \sum_{k=1}^{\bar{n}} \sum_{r=0}^p \Phi_{r+p(k-1)}^h(x_s) N_{r+p(k-1)}^p(x_f), \quad (16)$$

where  $N_{\mu}^p(x_f)$  are local functions, and  $\Phi_{\mu}^h(x_s)$  are node values of  $\Phi(x_{\mu}^f; x_s)$ . The local functions  $N_{\mu}^p(x_f)$  are piece-wise polynomials of the given order,  $p$  equals one only in the node  $x_{\mu}^f$  and equals zero in all other nodes  $x_{\nu}^f \neq x_{\mu}^f$  of the grid  $\Omega_{h^f(x_f)}^p(x_s)$ , i.e.,  $N_{\nu}^p(x_{\mu}^f) = \delta_{\nu\mu}$ ,  $\mu, \nu = 0, 1, \dots, \bar{n}p$ . The coefficients  $\Phi_{\nu}(x_s)$  are formally connected with the solution  $\Phi(x_{k,r}^{fp}; x_s)$  in a node  $x_{\nu}^f = x_{k,r}^{fp}$ ,  $k = 1, \dots, \bar{n}$ ,  $r = 0, \dots, p$ :

$$\Phi_{\nu}^h(x_s) = \Phi_{r+p(k-1)}^h(x_s) \approx \Phi(x_{k,r}^{fp}; x_s), \quad x_{k,r}^{fp} = x_{k-1}^f + \frac{h_k^f}{p} r.$$

The theoretical estimate for the  $\mathbf{H}^0$  norm between the exact and numerical solution has the order of

$$|\check{\lambda}_j(x_s) - \check{\lambda}_j^h(x_s)| \leq c_1 h^{2p}, \quad \left\| \Phi_j(x_f; x_s) - \Phi_j^h(x_s) \right\|_0 \leq c_2 h^{p+1}, \quad (17)$$

where  $h^f = \max_{1 < j < \bar{n}} h_j^f$  is the maximal step of the grid, and the constants  $c_1 > 0$ ,  $c_2 > 0$  do not depend on the step  $h^f$  [19]. It has been shown possible to construct schemes for solving the BVPs and integrals with high order of accuracy comparable with that of the computer in accordance with the following estimations [13]

$$\left| \frac{\partial \check{\lambda}_j(x_s)}{\partial x_s} - \frac{\partial \check{\lambda}_j^h(x_s)}{\partial x_s} \right| \leq c_3 h^{2p}, \quad \left\| \frac{\partial \Phi_j(x_f; x_s)}{\partial x_s} - \frac{\partial \Phi_j^h(x_s)}{\partial x_s} \right\|_0 \leq c_4 h^{p+1}, \quad (18)$$

$$|Q_{ij}(x_s) - Q_{ij}^h(x_s)| \leq c_5 h^{2p}, \quad |W_{ij}(x_s) - W_{ij}^h(x_s)| \leq c_6 h^{2p}, \quad (19)$$

where  $h^f$  is the grid step,  $p$  is the order of finite elements,  $i, j$  are the numbers of the corresponding solutions, and the constants  $c_3$ ,  $c_4$ ,  $c_5$ , and  $c_6$  do not depend on the step  $h^f$ . The proof is straightforward following the scheme of the proof of estimations (17) in accordance with [19,20]. Verification of the above estimations is provided by numerical analysis on condensed grids and by comparison with examples of exact solvable models A and B.

Let us consider the reduction of BVP (9), (11) in the interval  $\Delta: x_{\min}^f(x_s) < x_f < x_{\max}^f(x_s)$  with the boundary conditions (10) at points  $x_{\min}^f(x_s)$  and  $x_{\max}^f(x_s)$  rewritten in the form

$$\mathbf{A}(x_s)\Phi_j(x_f; x_s) = \check{\lambda}_j(x_s)\mathbf{B}(x_s)\Phi_j(x_f; x_s), \quad (20)$$

where  $\mathbf{A}(x_s)$  is a differential operator, and  $\mathbf{B}(x_s)$  is a multiplication operator, differentiable with respect to the parameter  $x_s \in \Omega_{x_s}$ . Substituting the expansion (16) into (20) and performing integration with respect to  $x_f$  by parts in the interval  $\Delta = \cup_{k=1}^{\bar{n}} \Delta_k$ , we arrive at a set of linear algebraic equations

$$\mathbf{a}_{\mu\nu}^p(x_s)\Phi_{j,\mu}^h(x_s) = \check{\lambda}_j^h(x_s)\mathbf{b}_{\mu\nu}^p(x_s)\Phi_{j,\mu}^h(x_s), \quad (21)$$

in the framework of the briefly described FEM. Using the  $p$ -order Lagrange elements [19], we present below Algorithm 1 for constructing the algebraic problem (21) by the FEM in the form of conventional pseudocode. Its MAPLE realization allows us to show explicitly the recalculation of indices  $\mu, \nu$  and to test the corresponding modules of the parametric matrix problems, derivatives of solutions by parameter, and calculation of integrals.

**Algorithm 1.** Generation of parametric algebraic problems**Input:**

$\Delta = \cup_{k=1}^{\bar{n}} \Delta_k = [x_{\min}^f(x_s), x_{\max}^f(x_s)]$  is the interval of changing of the independent variable  $x_f$ , whose boundaries depend on the parameter  $x_s = x_{k'}^s$ ;

$h_k^f = x_k^f - x_{k-1}^f$  is the grid step;

$\bar{n}$  is the number of subintervals  $\Delta_k = [x_{k-1}^f, x_k^f]$ ;

$p$  is the order of finite elements;

$\mathbf{A}(x_s), \mathbf{B}(x_s)$  are the differential operators in Eq. (20);

**Output:**

$N_{\mu}^p(x_f)$  are the basis functions in (16);

$\mathbf{a}_{\mu\nu}^p(x_s), \mathbf{b}_{\mu\nu}^p(x_s)$  are the matrix elements in the system of algebraic equations (21);

**Local:**

$x_{k,r}^{fp}$  are the nodes;  $\phi_{k,r}^p(x_f)$  are the Lagrange elements;  $\mu, \nu = 0, 1, \dots, \bar{n}p$ ;

---



---

```

1: for k:=1 to  $\bar{n}$  do
    for r:=0 to p do
         $x_{k,r}^{fp} = x_{k-1}^f + \frac{h_k^f}{p}r$ 
    end for;
end for;
2:  $\phi_{k,r}^p(x_f) = \prod_{r' \neq r} [(x_f - x_{k,r'}^{fp})(x_{k,r}^{fp} - x_{k,r'}^{fp})^{-1}]$ 
3:  $N_0^p(x_f) :=$  if  $x_f \in \Delta_1$  then  $\phi_{1,0}^p(x_f)$  else 0;
   for k:=1 to  $\bar{n}$  do
       for r:=1 to p-1 do
            $N_{r+p(k-1)}^p(x_f) :=$  if  $x_f \in \Delta_k$  then  $\phi_{k,r}^p(x_f)$  else 0;
       end for;
        $N_{kp}^p(x_f) :=$  if  $x_f \in \Delta_k$  then  $\phi_{k,p}^p(x_f)$ 
           else if  $x_f \in \Delta_{k+1}$  then  $\phi_{k+1,0}^p(x_f)$  else 0;
       end for;
        $N_{\bar{n}p}^p(x_f) :=$  if  $x_f \in \Delta_{\bar{n}}$  then  $\phi_{\bar{n},p}^p(x_f)$  else 0;
4: for  $\mu, \nu := 0$  to  $\bar{n}p$  do
     $\mathbf{a}_{\mu\nu}^p(x_s) := \int_{\Delta} g_1(x_f) N_{\mu}^p(x_f) \mathbf{A}(x_s) N_{\nu}^p(x_f) dx_f$ ;
     $\mathbf{b}_{\mu\nu}^p(x_s) := \int_{\Delta} g_1(x_f) N_{\mu}^p(x_f) \mathbf{B}(x_s) N_{\nu}^p(x_f) dx_f$ ;
end for;
```

---



---

**Remarks:**

1. For equation (9), the matrix elements of the operator (7), and  $V(x_f; x_s) = \check{V}_{fs}(x_f, x_s) + \check{V}_f(x_f)$  between the local functions  $N_{\mu}(x_f)$  and  $N_{\nu}(x_f)$  defined in the same interval  $\Delta_j$  calculated by formula using  $x_f = x_{k-1}^f + 0.5h_k^f(1 + \eta_f)$ ,  $q, r = \bar{0}, \bar{p}$ :



$$\begin{aligned}
(\mathbf{a}(x_s))_{\mu,\nu} &= \int_{-1}^{+1} \left\{ \frac{4}{(h_k^f)^2} g_{2f}(x_f) (\phi_{k,q}^p)' (\phi_{k,r}^p)' + g_{1f}(x_f) V(x_f; x_s) \phi_{k,q}^p \phi_{k,r}^p \right\} \frac{h_k^f}{2} d\eta_f, \\
(\mathbf{b}(x_s))_{\mu,\nu} &= \int_{-1}^{+1} g_{1f}(x_f) \phi_{k,q}^p \phi_{k,r}^p \frac{h_k^f}{2} d\eta_f, \quad \mu = q + p(k-1), \quad \nu = r + p(k-1).
\end{aligned}$$

2. If the integrals can not be calculated analytically (see, e.g., section 4), then they are calculated by numerical methods [19], namely, by means of the Gauss quadrature formulae of the order  $p+1$ .

3. For OSQD&PSQD model C, the problem (9)–(11) has been solved using the grid  $\Omega_{h^f(x_f)}^p(x_s)[x_{\min}^f, x_{\max}^f] = -1(20)1$  (the number in parentheses denotes the number of finite elements of order  $p=4$  in each interval).

Generally, 10-16 iterations are required for the subspace iterations to converge the subspace to within the prescribed tolerance. If the matrix  $\mathbf{a}^p \equiv \mathbf{a}^p(x_s)$  in Eq. (21) is not positively defined, the problem (21) is replaced by the following problem:

$$\tilde{\mathbf{a}}^p \Phi^h = \tilde{\lambda}^h \mathbf{b}^p \Phi^h, \quad \tilde{\mathbf{a}}^p = \mathbf{a}^p - \alpha \mathbf{b}^p. \quad (22)$$

The number  $\alpha$  (the shift of the energy spectrum) is chosen in such a way that the matrix  $\tilde{\mathbf{a}}^p$  is positive. The eigenvector of the problem (22) is the same, and  $\tilde{\lambda}^h = \lambda^h + \alpha$ , where the shift  $\alpha$  is evaluated by Algorithm 2.

**Algorithm 2.** Evaluating the lower bound for the lowest eigenvalue of the generalized eigenvalue problem

Generally it is impossible to define the lower bound for the lowest eigenvalue of Eq. (22) because the eigenvalues  $\tilde{\lambda}_1^h(x_s) < \dots < \tilde{\lambda}_i^h(x_s) < \dots < \tilde{\lambda}_{j_{max}^h}^h(x_s)$  depend upon the parameter  $x_s$ . However, we can use the following algorithm to find the lower bound for the lowest eigenvalue  $\tilde{\lambda}_1^h(x_s)$  at a fixed value of  $x_s$ :

- Step 1.** Calculate  $\mathbf{LDL}^T$  factorization of  $\mathbf{A}^p - \alpha \mathbf{B}^p$ .
- Step 2.** If some elements of the diagonal matrix  $\mathbf{D}$  are less than zero then put  $\alpha = \alpha - 1$  and go to **Step 3**, else go to **Step 5**.
- Step 3.** Calculate  $\mathbf{LDL}^T$  factorization of  $\mathbf{A}^p - \alpha \mathbf{B}^p$ .
- Step 4.** If some elements of the diagonal matrix  $\mathbf{D}$  are less than zero then put  $\alpha = \alpha - 1$  and go to **Step 3**, else put  $\alpha = \alpha - 0.5$  and go to **Step 8**.
- Step 5.** Put  $\alpha = \alpha + 1$  and calculate  $\mathbf{LDL}^T$  factorization of  $\mathbf{A}^p - \alpha \mathbf{B}^p$ .
- Step 6.** If all elements of the diagonal matrix  $\mathbf{D}$  are greater than zero then go to **Step 5**.
- Step 7.** Put  $\alpha = \alpha - 1.5$ .
- Step 8.** End.

After using the above algorithm one should find the lower bound for the lowest eigenvalue, and always  $\tilde{\lambda}_1^h(x_s) - \alpha \leq 1.5$ .

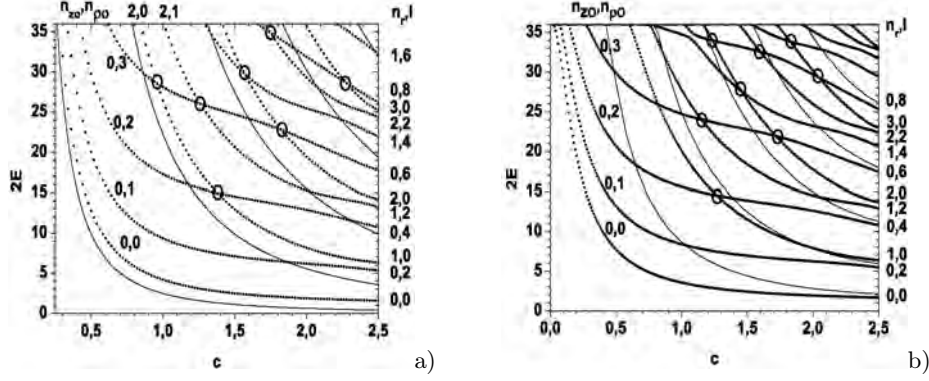


**Fig. 1.** The energies  $2E = \tilde{E}/E_R$  of even  $\sigma = +1$  lower states for OSQD versus the minor  $c$ ,  $\zeta_{ca} = c/a \in (1/5, 1)$  being the spheroid aspect ratio: a) well with impermeable walls, b) diffusion potential with  $2U_0 = 36$ ,  $s = 0.1$ , the major semiaxis  $a = 2.5$  and  $m = 0$ . Tine lines are minimal values  $2E_i^{min} \equiv 2E_i(x_s = 0)$  of potential curves.

## 4 Spectral Characteristics of Spheroidal QDs

**Models B and C for Oblate Spheroidal QD.** At fixed coordinate  $x_s$  of the slow subsystem, the motion of the particle in the fast degree of freedom  $x_f$  is localized within the potential well having the effective width

$$\tilde{L}(x_s) = 2c\sqrt{1 - x_s^2/a^2}, \quad (23)$$

where  $L = \tilde{L}/a_B^*$ . The parametric BVP (9)–(11) at fixed values of the coordinate  $x_s$ ,  $x_s \in (0, a)$ , is solved in the interval  $x_f \in (-L(x_s)/2, L(x_s)/2)$  for Model C using the program ODPEVP, and for Model B the eigenvalues  $\tilde{E}_{n_o}(x_s)/E_R \equiv 2E_i(x_s)$ ,  $n_o = i = 1, 2, \dots$ , and the corresponding parametric eigenfunctions  $\Phi_i^\sigma(x_f; x_s)$ , obeying the boundary conditions (10) and the normalization condition (11), are expressed in the analytical form:

$$2E_i(x_s) = \frac{\pi^2 n_o^2}{L^2(x_s)}, \quad \Phi_i^\sigma(x_f; x_s) = \sqrt{\frac{2}{L(x_s)}} \sin\left(\frac{\pi n_o}{2} \left(\frac{x_f}{L(x_s)/2} - 1\right)\right), \quad (24)$$

where the even solutions  $\sigma = +1$  are labelled with odd  $n_o = n_{zo} + 1 = 2i - 1$ , and the odd ones  $\sigma = -1$  with even  $n_o = n_{zo} + 1 = 2i$ ,  $i = 1, 2, 3, \dots$ . The effective potentials (13) in Eq. (12) for the slow subsystem are expressed analytically via the integrals over the fast variable  $x_f$  of the basis functions (24) and their derivatives with respect to the parameter  $x_s$  including states with both parities  $\sigma = \pm 1$ :

$$2E_i(x_s) = \frac{a^2 \pi^2 n_o^2}{4c^2(a^2 - x_s^2)}, \quad W_{ii}(x_s) = \frac{3 + \pi^2 n_o^2}{12} \frac{x_s^2}{(a^2 - x_s^2)^2}, \quad (25)$$

$$W_{ij}(x_s) = \frac{2n_o n'_o (n_o^2 + n'_o{}^2)(1 + (-1)^{n_o + n'_o})}{(n_o^2 - n'_o{}^2)^2} \frac{x_s^2}{(a^2 - x_s^2)^2},$$

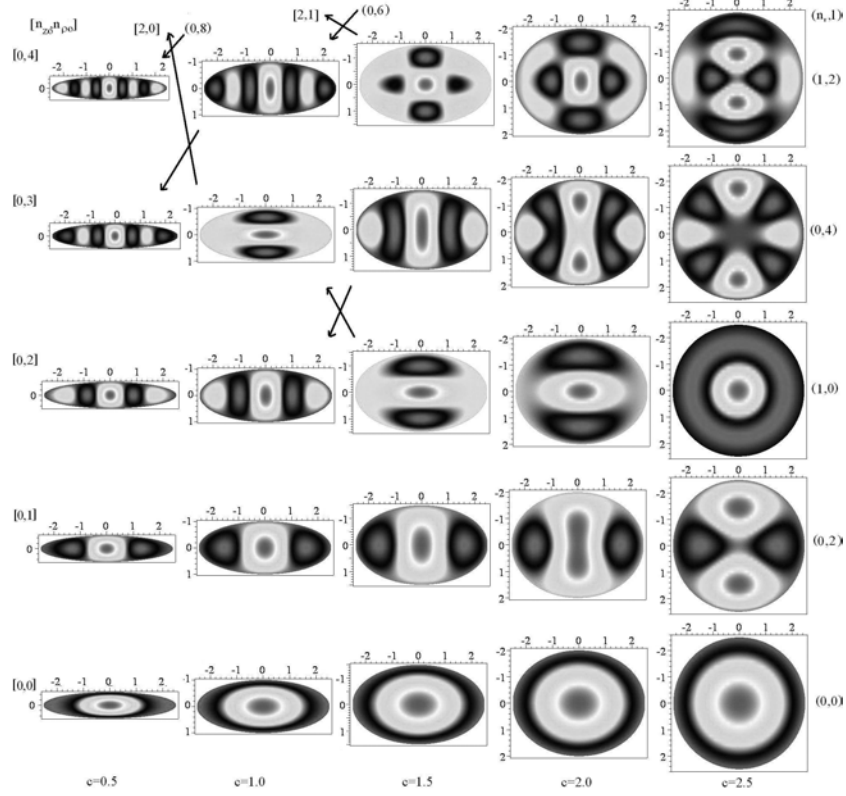


**Fig. 2.** Contour lines of the first five even-parity wave functions  $\sigma = +1$  in the  $xz$  plane of Model B of OSQD for the major semiaxis  $a = 2.5$  and different values of the minor semiaxis  $c$  ( $\zeta_{ca} = c/a \in (1/5, 1)$ )

$$Q_{ij}(x_s) = \frac{n_o n'_o (1 + (-1)^{n_o + n'_o})}{(n_o^2 - n'^o_2)^2} \frac{x_s}{a^2 - x_s^2}, \quad n'_o \neq n_o.$$

For Model B at  $c = a = r_0$  the OSQD turns into SQD with known analytically expressed energy levels  $E_t \equiv E_{nlm}^{sp}$  and the corresponding eigenfunctions

$$2E_{nlm}^{sp} = \frac{\alpha_{n_r+1, l+1/2}^2}{r_0^2}, \quad \Phi_{nlm}^{sp}(r, \theta, \varphi) = \frac{\sqrt{2} J_{l+1/2}(\sqrt{2E_{nlm}^{sp}} r)}{r_0 \sqrt{r} |J_{l+3/2}(\alpha_{n_r+1, l+1/2})|} Y_{lm}(\theta, \varphi), \quad (26)$$

where  $\alpha_{n_r+1, l+1/2}$  are zeros of the Bessel function of semi-integer index  $l + 1/2$ , numbered in ascending order  $0 < \alpha_{11} < \alpha_{12} < \dots < \alpha_{iv} < \dots$  by the integer  $i, v = 1, 2, 3, \dots$ . Otherwise one can use equivalent pairs  $iv \leftrightarrow \{n_r, l\}$  with  $n_r = 0, 1, 2, \dots$  numbering the zeros of Bessel function and  $l = 0, 1, 2, \dots$  being the orbital quantum number that determines the parity of states  $\hat{\sigma} = (-1)^l = (-1)^m \sigma$ ,  $\sigma = (-1)^{l-m} = \pm 1$ . At fixed  $l$ , the energy levels  $\tilde{E}_{nlm}/E_R = 2E_t$  degenerate with respect to the magnetic quantum number  $m$ , are labelled with

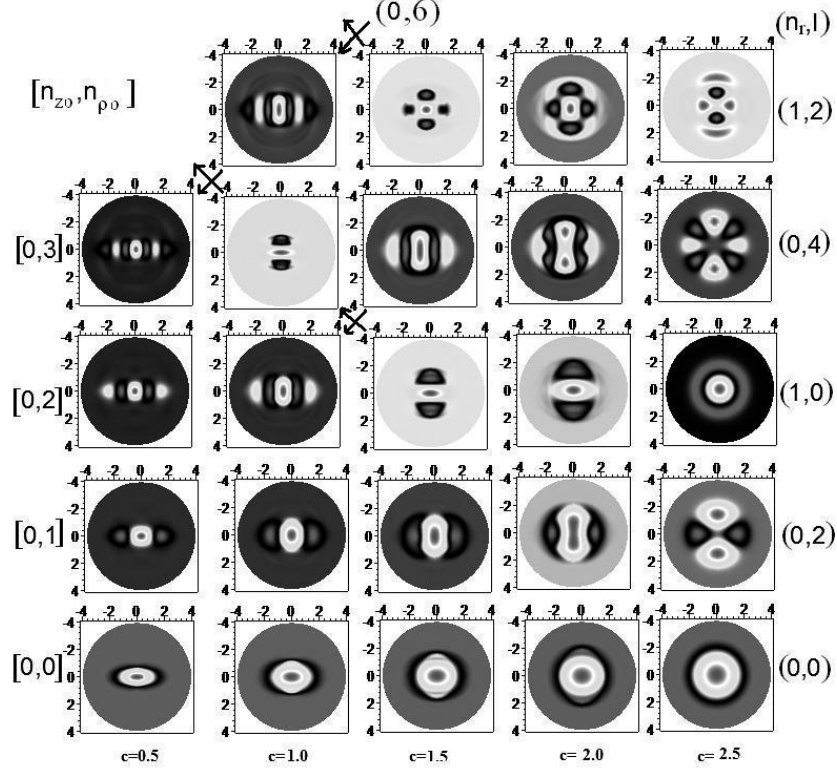


**Fig. 3.** Contour lines of the first five even-parity wave functions  $\sigma = +1$  in the  $xz$  plane of Model C of OSQD with  $2U_0 = 36$  and  $s = 0.1$  for the major semiaxis  $a = 2.5$  and different values of the minor semiaxis  $c$  ( $\zeta_{ca} = c/a \in (1/5, 1)$ )

the quantum number  $n = n_r + 1 = i = 1, 2, 3, \dots$ , in contrast to the spectrum of a spherical oscillator, degenerate with respect to the quantum number  $\lambda = 2n_r + l$ . Figures 1, 2, and 3 show the lower part of non-equidistant spectrum  $\tilde{E}(\zeta_{ca})/E_R = 2E_t$  and the eigenfunctions  $\Psi_t^{m\sigma}$  from Eq. (8) for even states OSQD Models B and C at  $m = 0$ . There is a one-to-one correspondence rule  $n_o = n_{zo} + 1 = 2n - (1 + \sigma)/2$ ,  $n = 1, 2, 3, \dots$ ,  $n_\rho = (l - |m| - (1 - \sigma)/2)/2$ , between the sets of spherical quantum numbers  $(n, l, m, \hat{\sigma})$  of SQD with radius  $r_0 = a = c$  and spheroidal ones  $(n_\xi = n_r, n_\eta = l - |m|, m, \sigma)$  of OSQD with the major  $a$  and the minor  $c$  semiaxes, and the adiabatic set of cylindrical quantum numbers  $(n_{zo}, n_\rho, m, \sigma)$  at continuous variation of the parameter  $\zeta_{ca} = c/a$ . The presence of crossing points of the energy levels of similar parity under the symmetry change from spherical  $\zeta_{ca} = 1$  to axial, i.e., under the variation of the parameter  $0 < \zeta_{ca} < 1$ , in the BVP with two variables at fixed  $m$  for Model B is caused by the possibility of variable separation in the OSC [17], i.e., the r.h.s. of Eq. (12) equals zero. The transformation of eigenfunctions occurring in the course of a transition through the crossing points (marked by circles) in Fig. 1, is shown in Fig. 2 for model B and in Fig. 3 for model C (marked by arrows). From

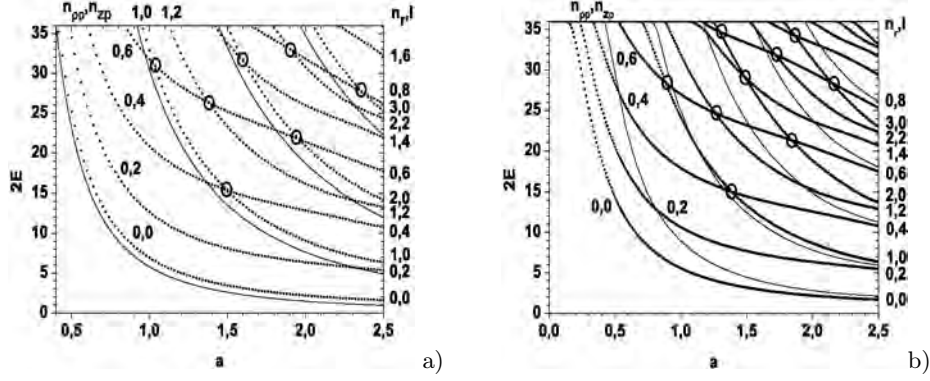


**Fig. 4.** The energies  $2E = \tilde{E}/E_R$  of even  $\sigma = +1$  lowest states for PSQD depending on the minor semiaxis  $a$  ( $\zeta_{ac} = a/c \in (1/5, 1)$  is the spheroid aspect ratio): a) well with impermeable walls, b) diffusion potential,  $2U_0 = 36$ ,  $s = 0.1$ , for the major semiaxis  $c = 2.5$  and  $m = 0$ . Tine lines are minimal values  $2E_i^{min} \equiv 2E_i(x_s = 0)$  of potential curves.

comparison of these Figures one can see that if the eigenfunctions are ordered according to increasing eigenvalues of the BVPs, then for both Models B and C, the number of nodes [18] is invariant under the variation of parameter  $c$  from  $c = a = 2.5$  to  $c = 0.5$  of potentials (3) and (4). For Model B, such a behavior follows from the fact of separation of variables of the BVP with potential (3) in the OSC (see Table 1), while for Model C, further investigation is needed because the coordinate system, where the variables of the BVP with potential (4) are separated, is unknown. So, at small value of deformation parameter ( $\zeta_{ca}$  for OSQD or  $\zeta_{ac}$  for PSQD) there are nodes only along corresponding major axis. For Model C, at each value of the parameter  $a$  their is a finite number of discrete energy levels limited by the value  $2U_0$  of the well walls height. As shown in Fig. 1b, the number of levels of OSQD, equal to that of SQD at  $a = c = r_0$ , is reduced with the decrease of the parameter  $c$  (or  $\zeta_{ca}$ ), in contrast to Models A and B that have countable spectra, and avoided crossings appear just below the threshold.

**Models B and C for Prolate Spheroidal QD.** In contrast to OSQD, for PSQD at fixed coordinate  $x_s$  of the slow subsystem the motion of the particle is confined to a 2D potential well with the effective variable radius

$$\rho_0(x_s) = a\sqrt{1 - x_s^2/c^2}, \quad (27)$$

where  $\rho_0(x_s) = \tilde{\rho}_0(x_s)/a_B$ . The parametric BVP (9)–(11) at fixed values of the coordinate  $x_s$  from the interval  $x_s \in (-c, c)$  is solved in the interval  $x_f \in (0, \rho_0(x_s))$  for Model C using the program ODPEVP, while for Model B the eigenvalues  $\tilde{E}_{n_{pp}+1}(x_s)/E_R \equiv 2E_i(x_s)$ ,  $n_{pp} + 1 = i = 1, 2, \dots$ , and the corresponding parametric basis functions  $\Phi_i^{m\sigma=0}(x_f; x_s) \equiv \Phi_i^m(x_f; x_s)$  without

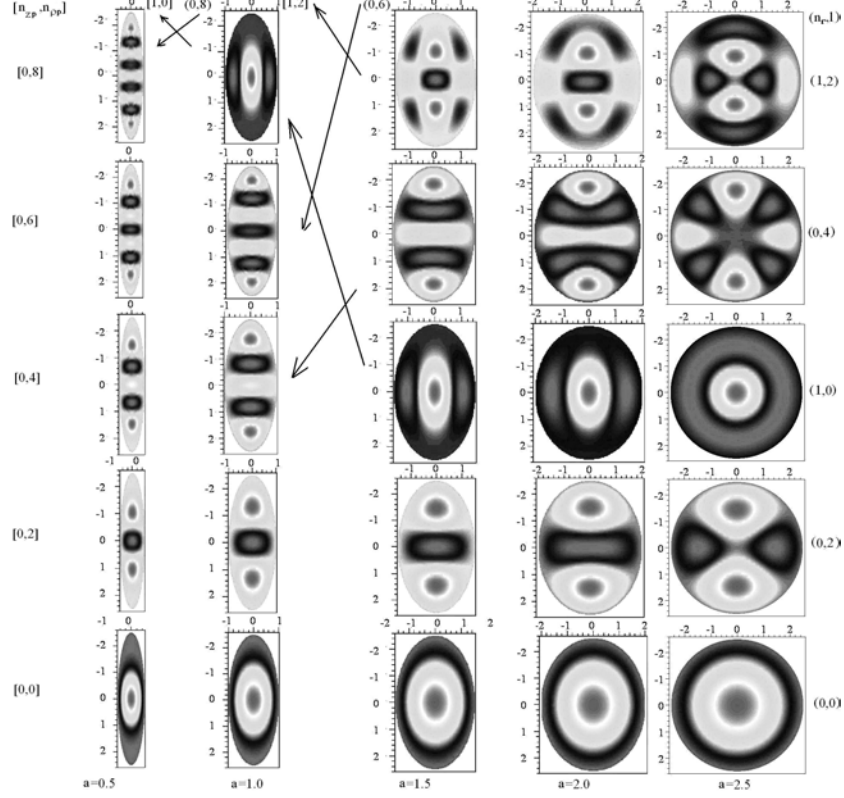


**Fig. 5.** Contour lines of the first five even-parity wave functions  $\sigma = +1$  in the  $xz$  plane of Model B of PSQD for the major semiaxis  $c = 2.5$  and different values of the minor semiaxis  $a$  ( $\zeta_{ac} = a/c \in (1/5, 1)$ )

parity separation obeying the boundary conditions (10) and the normalization condition (11) are expressed in the analytical form:

$$2E_i(x_s) = \frac{\alpha_{n_{pp}+1,|m|}^2}{\rho_0^2(x_s)}, \quad \Phi_{n_{pp}}^m(x_s) = \frac{\sqrt{2}}{\rho_0(x_s)} \frac{J_{|m|}(\sqrt{2E_{n_{pp}+1,|m|}}(x_s)x_f)}{|J_{|m|+1}(\alpha_{n_{pp}+1,|m|})|}, \quad (28)$$

where  $\alpha_{n_{pp}+1,|m|} = \tilde{J}_{|m|}^{n_{pp}+1}$  are positive zeros of the Bessel function of the first kind  $J_{|m|}(x_f)$  labeled in the ascending order with the quantum number  $n_{pp}+1 = i = 1, 2, \dots$ . The effective potentials (13) in Eq.(12) for the slow subsystem are calculated numerically in quadratures via the integrals over the fast variable  $x_f$  of the basis functions(28) and their derivatives with respect to the parameter  $x_s$  using SNA MATRA from Section 2. Figures 4 and 5 illustrate the lower part of the non-equidistant spectrum  $E(\zeta_{ac})/E_R = 2\tilde{E}_t$  and the eigenfunctions  $\Psi_t^{m\sigma}$  from Eq. (8) of even states of PSQD Models B and C. There is a one-to-one correspondence rule  $n_{pp} + 1 = n_p = i = n = n_r + 1$ ,  $i = 1, 2, \dots$  and  $n_{zp} = l - |m|$  between the sets of quantum numbers  $(n, l, m, \hat{\sigma})$  of SQD with the

radius  $r_0 = a = c$  and spheroidal ones ( $n_\xi = n_r, n_\eta = l - |m|, m, \sigma$ ) of PSQD with the major  $c$  and the minor  $a$  semiaxes, and the adiabatic set of quantum numbers ( $n = n_{\rho\rho} + 1, n_{z\rho}, m, \sigma$ ) under the continuous variation of the parameter  $\zeta_{ac} = a/c$ . The presence of crossing points of similar-parity energy levels in Fig. 4 under the change of symmetry from spherical  $\zeta_{ac} = 1$  to axial, i.e., under the variation of the parameter  $0 < \zeta_{ac} < 1$ , in the BVP with two variables at fixed  $m$  for Model B is caused by the possibility of variable separation in the PSC [17], i.e., r.h.s. of Eq. (12) equals zero. For Model C, at each value of the parameter  $c$  there is also only a finite number of discrete energy levels limited by the value  $2U_0$  of the well walls height. As shown in Fig. 4b, the number of energy levels of PSQD, equal to that of SQD at  $a = c = r_0$ , which is determined by the product of mass  $\mu_e$  of the particle, the well depth  $\tilde{U}_0$ , and the square of the radius  $\tilde{r}_0$ , is reduced with the decrease of the parameter  $\tilde{a}$  (or  $\zeta_{ac}$ ) because of the promotion of the potential curve (lower bound) into the continuous spectrum, in contrast to Models A and B having countable spectra. Note that the spectrum of Model C for PSQD or OSQD should approach that of Model B with the growth of the walls height  $U_0$  of the spheroidal well. However, at critical values of the ellipsoid aspect ratio it is shown that in the effective mass approximation, both the terms (lower bound) and the discrete energy eigenvalues in models of the B type move into the continuum. Therefore, when approaching the critical aspect ratio values, it is necessary to use models such as the lens-shaped self-assembled QDs with a quantum well confined to a narrow wetting layer [3] or if a minor semiaxis becomes comparable with the lattice constant to consider models (see, e.g. [21]), different from the effective mass approximation.

## 5 Conclusion

By examples of the analysis of energy spectra of SQD, PSQD, and OSQD models with three types of axially symmetric potentials, the efficiency of the developed computational scheme and SNA is demonstrated. Only Model A (anisotropic harmonic oscillator potential) is shown to have an equidistant spectrum, while Models B and C (wells with infinite and finite walls height) possess non-equidistant spectra. In Model C, there is a finite number of energy levels. This number becomes smaller as the parameter  $a$  or  $c$  ( $\zeta_{ac}$  or  $\zeta_{ca}$ ) is reduced because the potential curve (lower bound) moves into the continuum. Models A and B have countable discrete spectra. This difference in spectra allows verification of SQD, PSQD, and OSQD models using experimental data [2], e.g., photoabsorption, from which not only the energy level spacing, but also the mean geometric dimensions of QD may be derived [5,7,8]. It is shown that there are critical values of the ellipsoid aspect ratio, at which in the approximation of effective mass the discrete spectrum of models with finite-wall potentials turns into a continuous one. Hence, using experimental data, it is possible to verify different QD models like the lens-shaped self-assembled QDs with a quantum well confined to a narrow wetting layer [3], or to determine the validity domain of the effective mass approximation, if a minor semiaxis becomes comparable with the lattice constant and to proceed opportunely to more adequate models such as [21].

Note *a posteriori* that the diagonal approximation of the slow-variable ODE (12) without the diagonal matrix element  $W_{ii}$  (so-called rude adiabatic approximation) provides the lower estimate of the calculated energy levels. With this matrix element taken into account (adiabatic approximation), the upper estimate of energy is provided, unless in the domain of the energy level crossing points. Therefore, the Born–Oppenheimer (BO) approximation is generally applicable only for estimating the ground state at an appropriate value of the small parameter. For Model B in the first BO approximation  $2E_i \approx E_i^{(0)} + E_i^{(1)}$  is given by the minimal value of the slow subsystem energy  $E_1^{\min}(x_s)$  at the equilibrium points  $x_s = 0$  (namely,  $E_i^{(0)} = \pi^2 n_o^2 / (2c)^2$  from Eq. (24) for OSQD and  $E_i^{(0)} = \alpha_{n_{pp}+1}^2 / a^2$  from Eq. (28) for PSQD), and by the corresponding energy values  $E_i^{(1)} = \pi(ac)^{-1} n_o(2n_\rho + |m| + 1)$  and  $E_i^{(1)} = 2(ac)^{-1} \alpha_{n_{pp}+1, |m|} (n_z + 1/2)$  of the 2D and 1D harmonic oscillator, respectively. It is shown in [4] that the terms  $E_i(x_s)$  allow high-precision approximation by the Hulthén potential. This can be accomplished by means of computer algebra software, e.g., Maple, Mathematica, which allows (in the rude adiabatic approximation) to obtain the lower bound of the spectrum by solving transcendental equations expressed analytically in terms of known special functions, and to use this approach for further development of our SNA project.

The software package developed is applicable to the investigation of impurity and exciton states in semiconductor nanostructure models. Further development of the method and the software package is planned for solving the quasi-2D and quasi-1D BVPs with both discrete and continuous spectrum, which are necessary for calculating the optical transition rates, channeling and transport characteristics in the models like quantum wells and quantum wires.

Authors thank Profs. K.G. Dvovyan, E.M. Kazaryan, and H.A. Sarkisyan for collaboration in the field and Profs. T. Sturm and C. Philips for support of our SNA project. This work was done within the framework of the Protocol No. 3967-3-6-09/11 of collaboration between JINR and RAU in dynamics of finite-dimensional quantum models and nanostructures in external fields. The work was supported partially by RFBR (grants 10-01-00200 and 08-01-00604), and by the grant No. MK-2344.2010.2 of the President of Russian Federation.

## References

1. Harrison, P.: Quantum Well, Wires and Dots. In: Theoretical and Computational Physics of Semiconductor Nanostructures. Wiley, New York (2005)
2. Gambaryan, K.M.: Interaction and Cooperative Nucleation of InAsSbP Quantum Dots and Pits on InAs(100) Substrate. *Nanoscale. Res. Lett.* (2009), doi:10.1007/s11671-009-9510-8
3. Wojs, A., Hawrylak, P., Fafard, S., Jacak, L.: Electronic structure and magneto-optics of self-assembled quantum dots. *Phys. Rev. B* 54, 5604–5608 (1996)
4. Juharyan, L.A., Kazaryan, E.M., Petrosyan, L.S.: Electronic states and interband light absorption in semi-spherical quantum dot under the influence of strong magnetic field. *Solid State Comm.* 139, 537–540 (2006)
5. Dvovyan, K.G., Hayrapetyan, D.B., Kazaryan, E.M., Tshantshapanyan, A.A.: Electron States and Light Absorption in Strongly Oblate and Strongly Prolate Ellipsoidal Quantum Dots in Presence of Electrical and Magnetic Fields. *Nanoscale Res. Lett.* 2, 601–608 (2007)



6. Cantele, G., Ninno, D., Iadonisi, G.: Confined states in ellipsoidal quantum dots. *J. Phys. Condens. Matt.* 12, 9019–9036 (2000)
7. Trani, F., Cantele, G., Ninno, D., Iadonisi, G.: Tight-binding calculation of the optical absorption cross section of spherical and ellipsoidal silicon nanocrystals. *Phys. Rev. B* 72, 075423 (2005)
8. Lepadatu, A.-M., Stavarache, I., Ciurea, M.L., Iancu, V.: The influence of shape and potential barrier on confinement energy levels in quantum dots. *J. Appl. Phys.* 107, 033721 (2010)
9. Vinitsky, S.I., Gerdt, V.P., Gusev, A.A., Kaschiev, M.S., Rostovtsev, V.A., Samoilov, V.N., Tupikova, T.V., Chuluunbaatar, O.: A symbolic-numerical algorithm for the computation of matrix elements in the parametric eigenvalue problem. *Programming and Computer Software* 33, 105–116 (2007)
10. Chuluunbaatar, O., Gusev, A., Gerdt, V., Kaschiev, M., Rostovtsev, V., Samoylov, V., Tupikova, T., Vinitsky, S.: A Symbolic-numerical algorithm for solving the eigenvalue problem for a hydrogen atom in the magnetic field: cylindrical coordinates. In: Ganzha, V.G., Mayr, E.W., Vorozhtsov, E.V. (eds.) *CASC 2007. LNCS*, vol. 4770, pp. 118–133. Springer, Heidelberg (2007)
11. Chuluunbaatar, O., Gusev, A.A., Abrashkevich, A.G., Amaya-Tapia, A., Kaschiev, M.S., Larsen, S.Y., Vinitsky, S.I.: KANTBP: A program for computing energy levels, reaction matrix and radial wave functions in the coupled-channel hyperspherical adiabatic approach. *Comput. Phys. Commun.* 177, 649–675 (2007)
12. Chuluunbaatar, O., Gusev, A.A., Gerdt, V.P., Rostovtsev, V.A., Vinitsky, S.I., Abrashkevich, A.G., Kaschiev, M.S., Serov, V.V.: POTHMF: A program for computing potential curves and matrix elements of the coupled adiabatic radial equations for a hydrogen-like atom in a homogeneous magnetic field. *Comput. Phys. Commun.* 178, 301–330 (2008)
13. Chuluunbaatar, O., Gusev, A.A., Vinitsky, S.I., Abrashkevich, A.G.: ODPEVP: A program for computing eigenvalues and eigenfunctions and their first derivatives with respect to the parameter of the parametric self-adjointed Sturm-Liouville problem. *Comput. Phys. Commun.* 180, 1358–1375 (2009)
14. Vinitsky, S.I., Chuluunbaatar, O., Gerdt, V.P., Gusev, A.A., Rostovtsev, V.A.: Symbolic-numerical algorithms for solving parabolic quantum well problem with hydrogen-like impurity. In: Gerdt, V.P., Mayr, E.W., Vorozhtsov, E.V. (eds.) *CASC 2009. LNCS*, vol. 5743, pp. 334–349. Springer, Heidelberg (2009)
15. Kantorovich, L.V., Krylov, V.I.: *Approximate Methods of Higher Analysis*. Wiley, New York (1964)
16. Born, M., Huang, X.: *Dynamical Theory of Crystal Lattices*. The Clarendon Press, Oxford (1954)
17. Abramowitz, M., Stegun, I.A.: *Handbook of Mathematical Functions*. Dover, New York (1965)
18. Courant, R., Hilbert, D.: *Methods of Mathematical Physics*, vol. 1. Wiley, Chichester (1989)
19. Strang, G., Fix, G.J.: *An Analysis of the Finite Element Method*. Prentice-Hall, Englewood Cliffs (1973)
20. Schultz, M.H.:  $L^2$  Error Bounds for the Rayleigh-Ritz-Galerkin Method. *SIAM J. Numer. Anal.* 8, 737–748 (1971)
21. Harper, P.G.: Single Band Motion of Conduction Electrons in a Uniform Magnetic Field. *Proc. Phys. Soc. A* 68, 874–878 (1955)